REACTION RATE DISTRIBUTION MEASUREMENT AND THE CORE PERFORMANCE EVALUATION IN THE PROTOTYPE FBR MONJU

S. USAMI, Z. SUZUOKI, T. DESHIMARU

Monju Construction Office, Japan Nuclear Cycle Development Institute
2-1, Shiraki, Tsuruga-shi, Fukui-ken, 919-1279 Japan

F. NAKASHIMA

Tsuruga Head Office, Japan Nuclear Cycle Development Institute
65-20, kizaki, Tsuruga-shi, Fukui-ken, 919-1279 Japan

KEYWORDS : FBR – Reaction rate – Core breeding ratio – Power distribution

Introduction

Monju is a prototype fast breeder reactor designed to have an output of 280 MWe (714 MWt), fueled with mixed oxides of plutonium and uranium and cooled by liquid sodium. The principal data on plant design and performance are shown in Table 1.
Monju attained initial criticality in April 1994 and the reactor physics tests were carried out from May through November 1994. The reaction rate distribution measurement by the foil activation method was one of these tests and was carried out in order to verify the core performance and to contribute to the development of the core design methods. On the basis of the reaction rate measurement data, the Monju initial core breeding ratio and the power distribution were evaluated.

Reactor core description

The reactor core consists of 198 fuel assemblies surrounded by 172 radial blanket assemblies. The top and bottom parts of the fuel assemblies contain depleted uranium, forming axial blankets to the core. All fuel assemblies and all blanket assemblies are of identical overall size and have a hexagonal cross-section; they are 4.2 m long and weigh 200 kg each. The fuel assembly contains 169 pins and the blanket assembly 61 pins. These pins are filled with pellets of mixed oxide (MOX) and depleted uranium oxide, respectively. The neutron shield assemblies, made of stainless steel, are the same overall size as the fuel assemblies but contain no fuel. The core configuration and a fuel assembly are shown in Figures 1 and 2. To flatten the power distribution, the core is divided into two radial zones with different plutonium enrichment. In the initial core, the inner and outer zone have enrichments of 15% and 20% Pu-fissile/(Pu+U), respectively. The design average discharge burnup of the fuel is 80,000 MWD/T.
In-vessel storage racks are located around the reactor core within the reactor vessel.

The Reaction Rate Distribution Measurement

In the reaction rate distribution measurement by the foil activation method, several kinds of foils were used. Fission rates were measured with Pu-239, U-235, U-238 and

Table 1. Principal Design and Performance Data of Monju

- Reactor type : Sodium-cooled loop-type	- Cladding material : SUS316
- Thermal / Electrical output : 714 / 280 MW	- Cladding outer diameter / thickness : 6.5 / 0.47 mm
- Fuel material : PuO_2-UO_2	- Primary sodium temperature (reactor inlet / outlet) : 397 / 529 °C
- Core dimensions (equivalent diameter / height) : 1,790 / 930 mm	- Secondary sodium temperature (IHX inlet / outlet) : 325 / 505 °C
- Plutonium enrichment (inner core / outer core) :	- Reactor vessel (height / diameter) : 18 / 7 m
(Pu fissile %) Initial core 15 / 20	- Number of loops : 3
Equilibrium core 16 / 21	- Type of steam generator : Helical coil
- Blanket thickness (upper / lower / radial) : 30 / 35 / 30 cm	- Steam pressure / temperature (turbine inlet) : 12.7 MPa / 483 °C
- Fuel inventory : Core (U+Pu metal) 5.9 t	- Refueling system : Single rotating plug with fixed arm FHM
Blanket (U metal) 17.5 t	- Refueling interval : 6 months
- Average burnup at discharge : 80,000 MWD/T	
- Breeding ratio : 1.2	

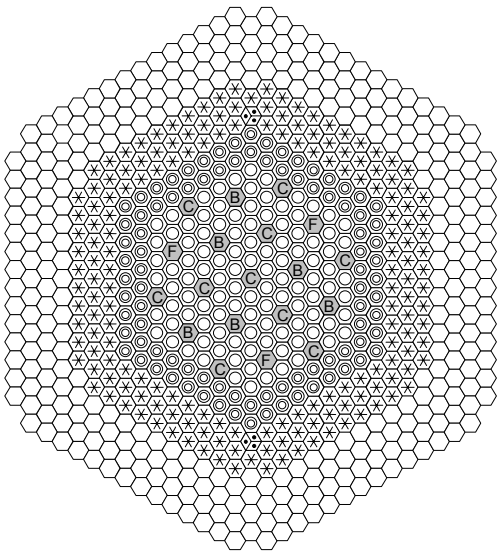

Core Zone	Inner Core	◯	108
	Outer Core	◎	90
Radial Blanket		✳	172
Control Rod	Fine Control Rod	F	3
	Coarse Control Rod	C	10
	Buckup Control Rod	B	6
Neutron Source		◈	2
Neutron Shield		⬡	324

Figure 1. Core Configuration

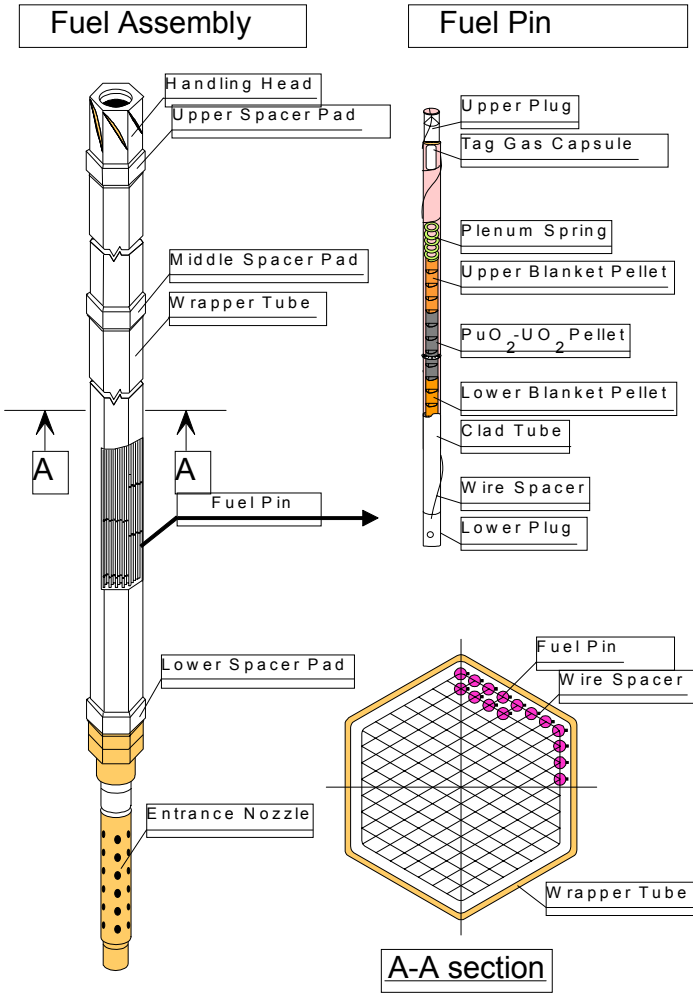

Figure 2. Fuel Assembly and Pin

Np-237 foils. Activation foils of Ni, Ti and Fe(Fe-54) were used to measure the neutron flux at high energy and foils of Au, Fe(Fe-58), Co, Sc and Na were used to measure the neutron flux at lower energies. The total number of Pu-239, U-235, U-238, Np-237 foils was 975, and that of the all types of foils was more than two thousand. The specification of foils is shown in Table 2. Each of the Pu-239, U-235, U-238, Sc and Na foils was wrapped in thin aluminum sheet.

Table 2. Specification of Foils

Foil	Type	Purity	Enrichment	Content per foil	Size (mm)	
					Diameter	Thickness
Pu-239	Pu-Al alloy	14% (Pu)	~98% (Pu-239)	~3.6mg (Pu-239)	7.0	0.2
U-235	U-Al alloy	15% (U)	~93% (U-235)	~3.3mg (U-235)	7.0	0.2
U-238	U-238 metal	100% (U)	~100% (U-238)	~165mg (U-238)	7.3	0.2
Np-237	NpO_2 grain	88% (Np)	~100% (Np-237)	~22mg (Np-237)	5	5
					(Zircaloy-4 Capsuled)	

Foil		Au	Ni	Ti	Fe	Co	Sc	Na(NaCl)
Size (mm)	Diameter	6.5	7.5	7.5	7.5	7.5	7.3	7.4
	Thickness	0.05	1.0, 3.0	1.0	1.0	0.5	0.5	3

The foils were placed at representative positions in the core region, the blanket region, the neutron shield region as well as the in-vessel storage racks by the use of special experimental assemblies. The structure of the experimental fuel assembly is shown in Figure 3. The experimental assemblies, which have the same basic structure as normal assemblies, were loaded in place of standard core elements. The foils were contained in a special detector pin located at the center of the pin bundle. In this detector pin, the outer diameter of which was 13 mm or 10 mm, stainless steel dummy pellets were used to space the foils at selected axial positions. Different foils were irradiated by exchanging the detector pin of the experimental assembly.

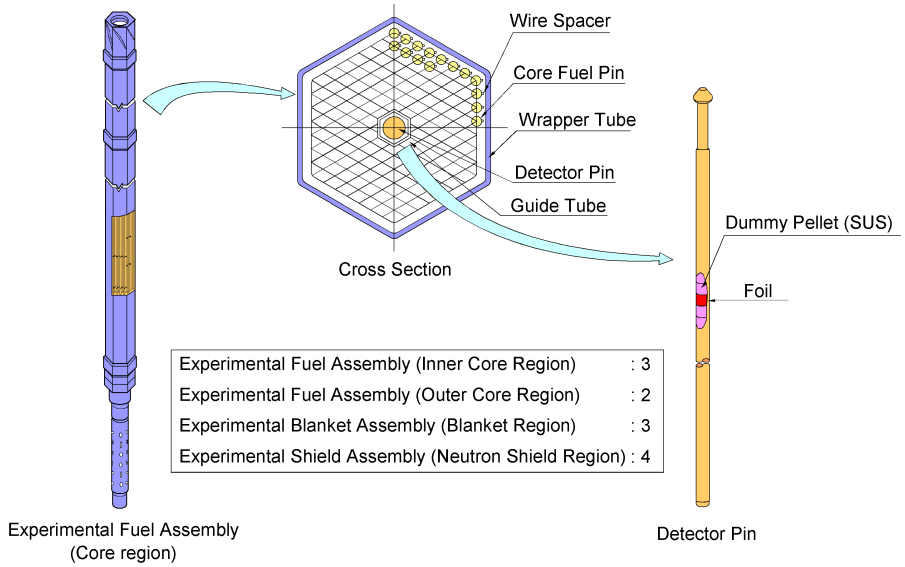

Figure 3. Experimental Fuel Assembly

Figure 4 shows the handling procedure for the experimental assemblies, the detector pins and the foils. After irradiation in the core, the experimental assembly with the detector pin was transferred to the fuel inspection facility. Here, the irradiated detector

pin was exchanged for a new unirradiated one by the use of the detector pin handling equipment. The experimental assembly was then reinserted into the core. The irradiated detector pin was cut in the glove box and the irradiated foils were removed. Then, the gamma-ray spectra of the irradiated foils were measured and the reaction rates were evaluated.

The irradiation of the experimental assemblies was carried out in six campaigns (P1~P6) at reactor powers ranging from 0.02~0.16% of rated power. The assemblies were irradiated in different locations and with different control rod configurations, the temperature being 200°C throughout the tests. The irradiation pattern of the experimental assemblies is shown in Figure 5. The irradiation time was 2 hours (P1~P5) or 4 hours (P6). The irradiation pattern was selected to cover almost an entire 30° sector of the core considering the geometrical symmetry of the core. The control

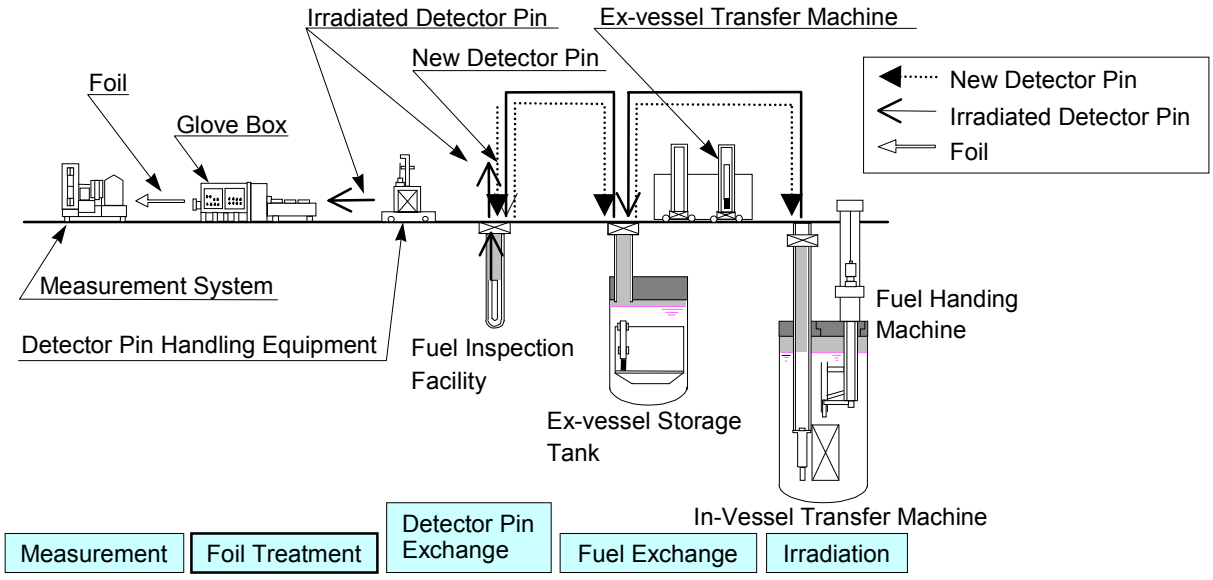

Figure 4. Handling Procedure for Experimental Assembly, Detector Pin, Foil

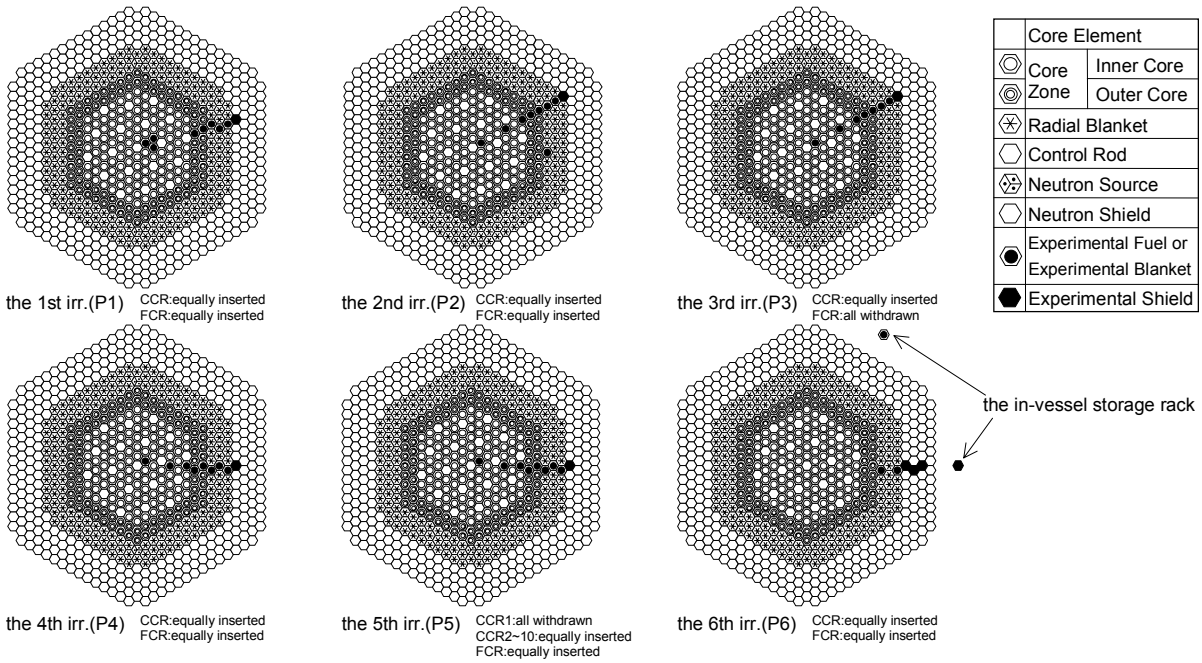

Figure 5. Irradiation Pattern of Experimental Assemblies

rods in each of the four irradiations P1, P2, P4, P6 were about 1/3 equally inserted. In both P2 and P3 measurements were made along a diagonal radius of the core, but in P3 all of the FCRs (fine control rods) were fully withdrawn. In irradiations P4 and P5 the measurements were made along a sideways radius of the core, but in P5 the CCR (coarse control rod) at the core center was fully withdrawn. In P6, measurements were made both in the shielding region and in the in-vessel storage racks by increasing the irradiation power and the irradiation time. As an example, the foil locations in the irradiation P2 are shown in Figure 6. In these six irradiations (P1~P6), a total of 51 detector pins and 2015 foils were irradiated.

The gamma ray spectra of the irradiated foils were measured by use of high purity Ge solid state detectors in the measurement system. This measurement system made it possible to count the large quantities of foils. The detector was precisely calibrated with the standard gamma ray sources whose gamma ray energies cover those of activated nuclides. Each foil was counted several times with the measurement system. This provided sufficient data to perform some valid statistical analyses. The measurements of the gamma rays from the foil were corrected for the pile-up effect, the coincidence summing effect, the foil shape effect for the detector efficiency, the self-shielding effect for the gamma ray in the foil, etc.. By considering the history of the irradiation and the conditions of the measurement, several types of reaction rate data were obtained from the gamma ray spectrum analyses: the fission rates of the fission foils and the capture rates of the U-238 foils were measured on the basis of the 1596.5 keV gamma ray of Ba(La)-140 fission product [1] and the 277.6 keV gamma ray of Np-239, respectively. Another correction was made for fissions of other nuclides in foils, such as U-235 in the U-238 foils. As a result, important basic data concerning the nuclear properties were collected, such as the reaction rate distributions and the reaction rate ratios in the initial core of Monju. As an example of the measured reaction rate distributions, the relative radial distribution of the measured Pu-239 fission rate (F9) on the core central plane is shown in Figure 7. The measured reaction rate ratio of U-238 capture rate to Pu-239 fission rate (C8/F9) at the core center was about 0.164~0.167.

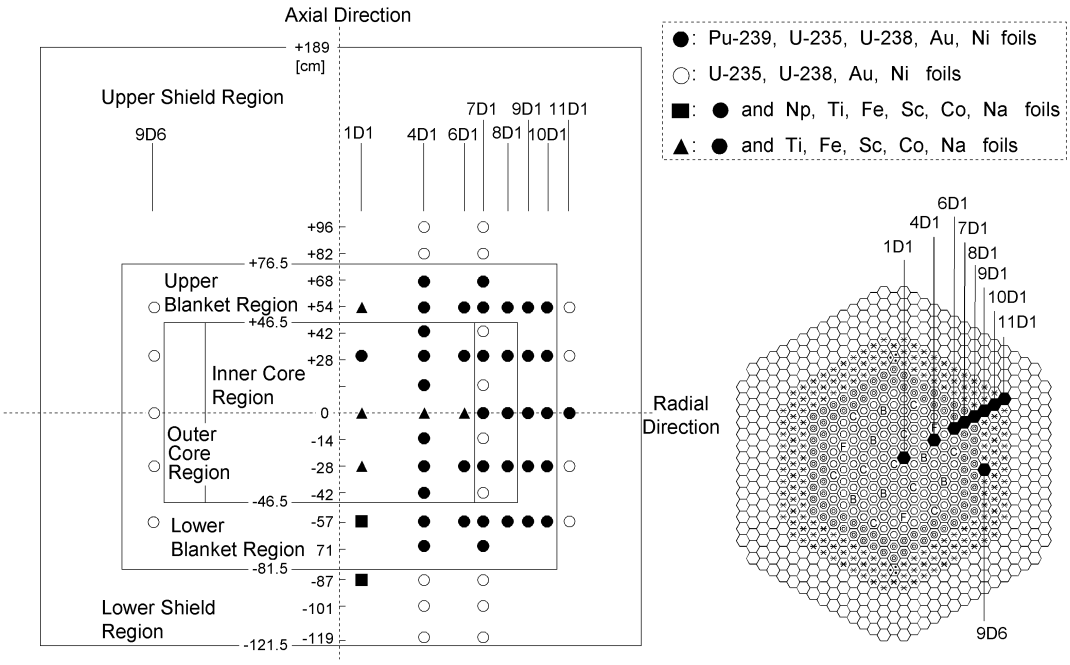

Figure 6. Foil Location in the Second Irradiation (P2)

The errors in gamma ray photo peak counts of foils, foil masses, isotopic compositions, half-lives, etc. were considered in the uncertainties of the measured relative reaction rate distributions which were normalized by the measured reaction rates at the core center. For example, the uncertainty in the F9 relative distribution from the core to the in-vessel storage rack was in the range of 0.7~2.2%. Furthermore, by considering the errors in gamma ray photo peak efficiencies, fission yields and gamma ray branching ratios, the uncertainty of the absolute reaction rates at the core center were obtained. For example, the uncertainties of the absolute values of F9 and C8 at the core center were about 2.5% and 5.6%, respectively. The main contribution to the uncertainty of the absolute value of C8 is the error in the branching ratio of the 277.6 keV gamma ray of Np-239 which was estimated to be 4.2% [2].

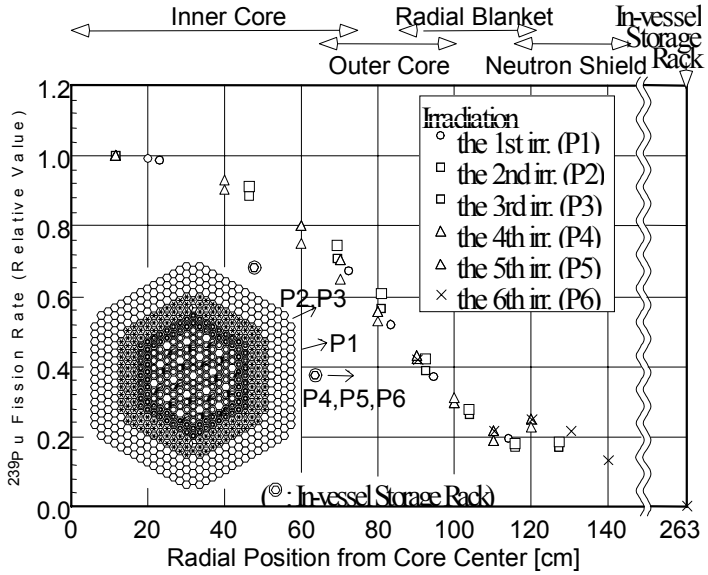

Figure 7. Radial Distribution of Measured Pu-239 Fission Rate on the Core Central Plane

The Reaction Rate Distribution Analysis

A detailed calculation of the reaction rates in the experimental assembly loading patterns (P1~P6) was carried out. Figure 8 shows the reaction rate analysis method. In the calculation of the reaction rates, diffusion theory was applied to the basic calculations of the neutron flux, which used JFS-3-J3.2 [3] and JFS-3-J2 [4] as the 70 group constants sets based on the JENDL-3.2 [5] library (referred to as J3.2 hereafter) and the JENDL-2 [6] library (referred to as J2 hereafter) and used the DIF3D code [7] with the Tri-Z calculation system of the full reactor model. Considering the effective cross sections of the foils, which were evaluated from the cell calculation by the SLAROM code [8] with the isolated lump approximation method, we obtained the calculated reaction rate and the C/E value of each reaction rate at each measurement position. The following corrections were also applied:

- the transport correction for the neutron flux distribution
- the correction for the heterogeneity inside the experimental assembly

Figure 9 shows the C/E values of the normalized Pu-239 fission rate (F9) radial distributions on the core central plane. It can be seen that the measurements and the calculations were in good agreement in the core region, but in both the radial blanket region and the neutron shield region, the C/E values were less than 1.0. Such a tendency was seen in the MOZART experiments of ZEBRA and the JUPITER

experiments of ZPPR. Concerning the ratio of U-238 capture rate to Pu-239 fission rate (C8/F9) at the core center of Monju, the C/E values were about 1.00~1.02. These results were the same as those of the FCA experiments [9], but not the same as the results of the MOZART experiments and the JUPITER experiments (the C/E values of C8/F9 in MOZART and JUPITER were about 1.05).

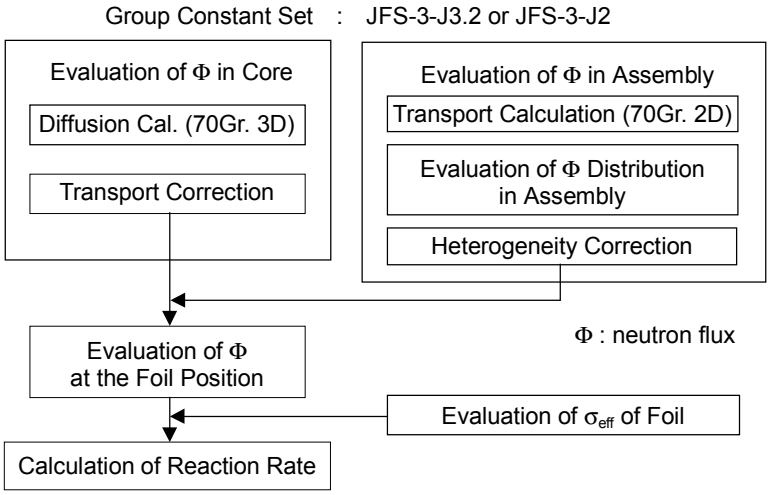

Figure 8. Reaction Rate Analysis Method

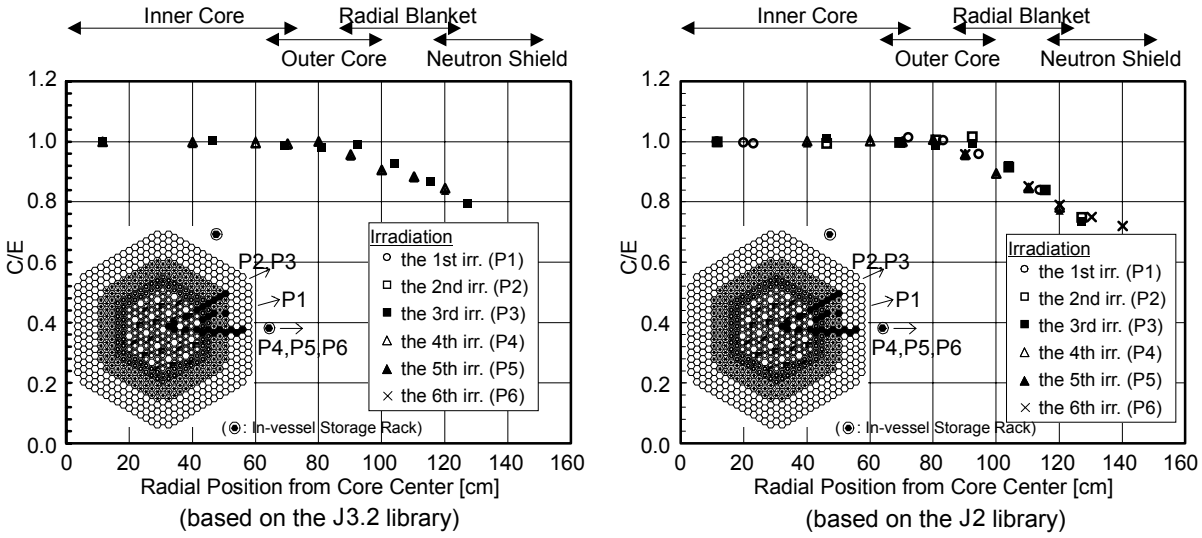

Figure 9. Radial Distribution of C/E of Pu-239 Fission Rate on the Core Central Plane

Evaluation method of the breeding ratio and the power distribution

The Monju initial core breeding ratio and the power distributions were evaluated by the use of the measured reaction rates of Pu-239(n,f), U-235(n,f), U-238(n,f), U-238(n,γ) and the calculated reaction rates of Pu-238(n,γ), Pu-240(n,γ), Pu-241(n,f), etc. and the calculated α-values (the ratio of capture rate to fission rate) of Pu-239, Pu-241, U-235. This calculation was based on the library of J3.2 or J2 and the DIF3D code with the Tri-Z calculation system of the full reactor model.

The breeding ratio (B.R.) was defined as follows:

$$B.R.= \frac{\text{production rate of fissile nuclide(capture rate of U-238, Pu-239, Pu-238)}}{\text{disappearance rate of fissile nuclide(absorption rate of Pu-239, Pu-241, U-235)}}$$

$$= \frac{\int_{reactor} dV\ [N_{28}<\sigma_{c28}\Phi> + N_{40}<\sigma_{c40}\Phi> + N_{48}<\sigma_{c48}\Phi>]}{\int_{reactor} dV\ [N_{49}<\sigma_{a49}\Phi> + N_{41}<\sigma_{a41}\Phi> + N_{25}<\sigma_{a25}\Phi>]}$$

$$= \zeta \times \xi_1 \times \frac{C_8(0)}{F_9(0)} \times \frac{\int_{reactor} dV\ [N_{28}\times\beta_1(r)\times C_8(r) + N_{40}\times\{C_0(0)/C_8(0)\}\times C_0(r) + N_{48}\times\{C_{48}(0)/C_8(0)\}\times C_{48}(r)]}{\int_{reactor} dV\ [N_{49}\times\beta_2(r)\times F_9(r)\times(1+\alpha_9) + N_{41}\times\{F_1(0)/F_9(0)\}\times F_1(r)\times(1+\alpha_1) + N_{25}\times\xi_3\times\{F_5(0)/F_9(0)\}\times\beta_3(r)\times F_5(r)\times(1+\alpha_5)]}$$

..... [1]

And the power density distribution (P(r)) was defined as follows:

$$\begin{aligned} P(r) &= \Sigma_{xe}\,[N_e(r) \times \{\kappa_{xe} \times R_{xe}(r) + \Sigma_g \Sigma_{g'} \sigma_{se,g\to g'} (E_g - E_{g'}) \Phi_g(r)\}] \\ &= \eta \times F_9(0) \times [N_{49}(r) \times \kappa_{f49} \times \beta_2(r) \times F_9(r) \\ &\quad + N_{25}(r) \times \kappa_{f25} \times \xi_3 \times \{F_5(0) / F_9(0)\} \times \beta_3(r) \times F_5(r) \\ &\quad + N_{28}(r) \times \kappa_{f28} \times \xi_4 \times \{F_8(0) / F_9(0)\} \times \beta_4(r) \times F_8(r) \\ &\quad + N_{28}(r) \times \kappa_{c28} \times \xi_1 \times \{C_8(0) / F_9(0)\} \times \beta_1(r) \times C_8(r) \\ &\quad + N_{41}(r) \times \kappa_{f41} \times \{F_1(0) / F_9(0)\} \times F_1(r) \\ &\quad + N_{48}(r) \times \kappa_{c48} \times \{C_{48}(0) / F_9(0)\} \times C_{48}(r) \\ &\quad + N_{40}(r) \times \kappa_{c40} \times \{C_0(0) / F_9(0)\} \times C_0(r) \\ &\quad + N_{etc}(r) \times \{\kappa_{f\,etc} \times F_{etc}(0) \times F_{etc}(r) + \kappa_{c\,etc} \times C_{etc}(0) \times C_{etc}(r)\} / F_9(0)] \\ &\quad + \Sigma_e\,[N_e(r) \times \{\Sigma_g \Sigma_{g'} \sigma_{se,g\to g'} (E_g - E_{g'}) \Phi_g(r)\} / F_9(0)] \end{aligned}$$

..... [2]

where

- $\sigma_{x\,e}$: microscopic cross section of nuclear reaction x in nuclide e
- Φ : neutron flux, $< \sigma_{x\,e}\ \Phi >$ shows the energy integration.
- $\Phi_g(r)$: neutron flux in the energy group g at the position r
- E_g : average neutron energy in the energy group g
- N_e : number density of nuclide e
- κ_{xe} : released energy per nuclear reaction x in nuclide e
- $R_{xe}(r)$: reaction rate of nuclear reaction x in nuclide e at the position r
- x : a (absorption = c + f), c (capture), f (fission), s (scattering)
- e : 25(U-235), 28(U-238), 48(Pu-238), 49(Pu-239), 40(Pu-240), 41(Pu-241), etc. (the others)
- $C_i(0)$: calculated capture rate of nuclide i at the core center
- $C_i(r)$: calculated relative distribution of capture rate of nuclide i at the position r in the core / blanket region
- $F_i(0)$: calculated fission rate of nuclide i at the core center
- $F_i(r)$: calculated relative distribution of fission rate of nuclide i at the position r in the core / blanket region
- α_i : α value of nuclide i
- i : 5 (U-235), 8 (U-238), 48 (Pu-238), 9 (Pu-239), 0 (Pu-240), 1 (Pu-241), etc. (the others)
- ζ : calculated correction factor for the effect of the power level (from the zero power to the rated power)

ξ_1, ξ_3, ξ_4 : E/C correction factor for the reaction rate ratio $C_8(0)/F_9(0)$, $F_5(0)/F_9(0)$, $F_8(0)/F_9(0)$ at the core center, respectively

η : E/C correction factor for the Pu-239 fission rate $F_9(0)$ at the core center [correction for the absolute value]

$\beta_1(r)$, $\beta_2(r)$, $\beta_3(r)$, $\beta_4(r)$: E/C correction factor for the reaction rate distribution $C_8(r)$, $F_9(r)$, $F_5(r)$, $F_8(r)$ at the position r, respectively

Concerning the correction factor for the γ-ray transport effect, the design values were used.

From the six loading patterns (P1~P6) of the experimental fuel assemblies in this test, the three patterns (P1, P2, P4), which covered almost an entire 30° sector of the core and in which the control rod positions were almost equal, were chosen for the evaluation. In order to evaluate the breeding ratio and the power distributions on the basis of the reaction rate measurement data, first of all, a detailed calculation of the reaction rates in the experimental fuel assembly loading patterns was carried out.

After the C/E values of the reaction rates in the foil loading positions were obtained, the C/E values of the reaction rates in the other positions of the core, which had no measurements, were estimated from the previous C/E values on the basis of the Akima's interpolation method [10]. By considering the geometrical symmetry of the core, the C/E values of the reaction rates were extended to the full core region. In the axial direction, the C/E value was estimated at each mesh point of a calculation. These C/E values of the reaction rates were used to correct the calculated reaction rates (where no experimental assemblies are loaded). By spatially integrating the corrected reaction rates, an evaluation of the breeding ratio and the power distributions was obtained.

Evaluation results of the breeding ratio

After the E/C correction factors for the reaction rate ratio $C_8(0)/F_9(0)$ and for the reaction rate distributions $C_8(r)$, $F_9(r)$, $F_5(r)$, i.e., ξ, $\beta_1(r)$, $\beta_2(r)$, $\beta_3(r)$ were obtained, these correction factors were used to correct the calculated reaction rates in the operating core on the basis of equation [1]. Applying the factor ζ (=1.02), which is the calculated correction factor for the effect of the power level (from the zero power to the rated power), we obtained 1.183 ~ 1.185 as the breeding ratio of the operating core at full power. The uncertainty of the evaluated breeding ratio was about 10% because the uncertainty of the measured reaction rate ratio $C_8(0)/F_9(0)$ and that of the measured reaction rate distribution were about 6% and 1%, respectively.

Table 3-1 and Table 3-2 show the results of the breeding ratio in each core region at full power. The calculated breeding ratios were in good agreement with the evaluated values.

Table 3-1. Results of the Breeding Ratio in Each Core Region at Full Power (based on the J3.2 library)

Region	Inner Core	Outer Core	Axial Blanket	Radial Blanket
Evaluated breeding ratio from the measurement	0.399	0.208	0.217	0.361
	0.607		0.578	
	1.185			
Calculated breeding ratio	0.402	0.209	0.208	0.385
	0.611		0.593	
	1.204			

Table 3-2. Results of the Breeding Ratio in Each Core Region at Full Power (based on the J2 library)

Region	Inner Core	Outer Core	Axial Blanket	Radial Blanket
Evaluated breeding ratio from the measurement	0.397	0.207	0.218	0.361
	0.604		0.579	
	1.183			
Calculated breeding ratio	0.399	0.207	0.201	0.373
	0.606		0.574	
	1.180			

Evaluation results of the power distribution

The E/C correction factors for the Pu-239 fission rate $F_9(0)$ and for the reaction rate ratios $C_8(0)/F_9(0)$, $F_5(0)/F_9(0)$, $F_8(0)/F_9(0)$ and for the reaction rate distributions $C_8(r)$, $F_9(r)$, $F_5(r)$, $F_8(r)$, i.e., η, ξ_1, ξ_3, ξ_4, $\beta_1(r)$, $\beta_2(r)$, $\beta_3(r)$, $\beta_4(r)$ were used to correct the calculated reaction rates in the operating core on the basis of equation [2]. It is considered that the energy loss of neutrons due to the scattering contributes to the heat generation. As a result, the power density distributions were obtained.

Integrating the power density distribution of each fuel assembly in the axial direction and multiplying it by the cross section of the assembly, the integrated power for each assembly was obtained. Figure 10 represents the integrated power for each assembly in the radial direction of the core. From Figure 10, the calculated and evaluated power distributions agree very well, and the flattening of the power distribution was attained effectively.

Table 4 shows the results of the ratio of the power generated in each core region. From Table 4, these were in good agreement between the calculation and the evaluation.

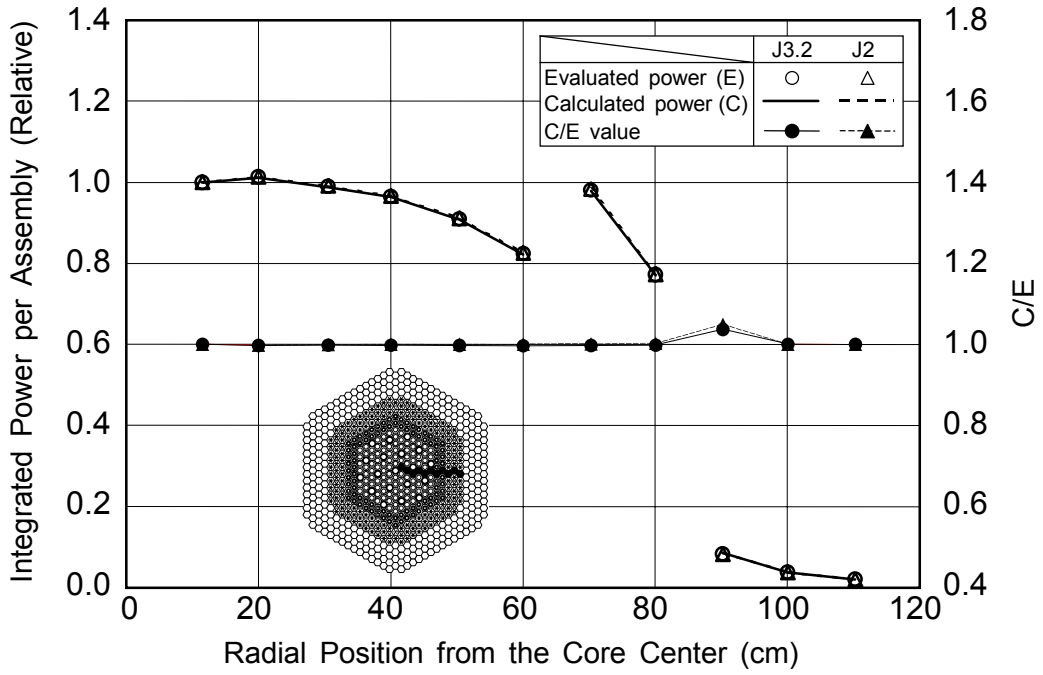

Figure 10. Radial Distribution and C/E Values of Integrated Power per Assembly

Table 4-1. Results of the Ratio of the Power in Each Core Region

Region		Ratio of the power in each core region			
		Inner Core	Outer Core	Radial Blanket	Axial Blanket
J3.2 Library	Evaluated value	0.539	0.403	0.0376	0.0205
		0.942		0.0581	
	Calculated value	0.539	0.403	0.0383	0.0196
		0.942		0.0579	
J2 Library	Evaluated value	0.539	0.403	0.0376	0.0204
		0.942		0.0580	
	Calculated value	0.538	0.404	0.0384	0.0195
		0.942		0.0579	

The axial peaking factor (F_Z) is defined as the ratio of the axial maximum power density to the axial average power density in an assembly. The radial peaking factor (F_{XY}) is given as the ratio of the maximum value of the integrated power per assembly over the core height to the averaged value of the integrated power per assembly over the core height in the inner and outer core region. The results of the peaking factors, which were evaluated by using of the power density distributions, are shown in Table 5. From Table 5, the calculated and evaluated peaking factors agreed very well.

Table 5. Results of the Peaking Factor (based on the J3.2 or J2 library)

	Radial peaking factor (F_{XY})		Axial peaking factor(F_Z)					
			Inner Core inner most row		Outer Core inner most row		Radial Blanket inner most row	
Library	J3.2	J2	J3.2	J2	J3.2	J2	J3.2	J2
Evaluated value	1.20	1.20	1.32	1.32	1.31	1.31	1.87	1.87
Calculated value	1.20	1.19	1.33	1.33	1.31	1.32	1.90	1.90

The maximum linear heat rating was evaluated on the basis of the power density distribution. The maximum linear heat rating (q_{max}) is defined as follows:

$$q_{max} = \frac{P_{core}}{H_{core} \times N_{pin}} \times F_Z \times f_{XY} \times \theta \quad \cdots\cdots\cdots\cdots [3]$$

where

H_{core} : core height (93 cm for core region)

N_{pin} : number of pins per assembly (169 for fuel assembly)

P_{core} : integrated power per assembly over the core height H_{core}
(The total power of the all regions was normalized by 714 MWt.)

F_Z : axial peaking factor in the core height H_{core}

θ : the correction factor for the axial elongation and the heating of wrapper tube from 200°C to the rated temperature, 0.9825 for the inner core fuel assembly and 0.9836 for the outer core fuel assembly (design value)

f_{XY} : calculated radial peaking factor inside the assembly

Table 6 shows the results of the maximum linear heat rating. From Table 6, the maximum linear heat rating was less than the design maximum value 360 W/cm, and the calculated and evaluated maximum linear heat rating of the core region were agreed to within 1%.

Table 6. Results of the Maximum Linear Heat Rating (based on the J3.2 or J2 library)

	Maximum liner heat rating (W/cm)			
	Inner Core		Outer Core	
Library	J3.2	J2	J3.2	J2
Evaluated value	330	329	334	335
Calculated value	331	330	336	338

Conclusion

Several types of reaction rates were measured with a total of 2015 foils in the initial core of the prototype FBR Monju, and important basic data concerning the nuclear properties were collected. Good agreement between the measurement and the calculation (based on the J3.2 library, the J2 library as well as the DIF3D code with the Tri-Z calculation system of the full reactor model) was obtained for the reaction rate radial distributions in the core region.

The Monju initial core breeding ratio and the power distribution were evaluated on the basis of the reaction rate measurement data. The results were as follows:

- The breeding ratio of the operating core at full power was approximately 1.18. The calculated breeding ratio was in good agreement with the evaluated value.
- The flattening of the power distribution was attained effectively. The calculated and evaluated power distributions agreed very well.
- Good agreement between the evaluation and the calculation was obtained for the ratio of the power in each core region, the peaking factor and the maximum linear heat rating.

As a result, it was verified that the core performance of Monju and the methods of core calculations were satisfactory.

References

1. K.Tasaka, et al., "JNDC Nuclear Data Library of Fission Products : Second Version," JAERI 1320, JAERI (1990).
2. E.Browne and R.B.Firestone, "Table of Radioactive Isotopes," Lawrence Berkeley Lab. Univ. of California (1986)
3. H.Takano, "Benchmark Tests of JENDL-3.2 for Thermal and Fast Reactors," in Proc. International Conference on Nuclear Data for Science and Technology, May 9-13, 1994, Gatlinburg, Tennessee USA, p809.
4. H.Takano, "Revised Edition of Fast Reactor Group Constant Set JFS-3-J2", JAERI-M 89-141, JAERI (1989).
5. T.Nakagawa, et al., "Japanese Evaluated Nuclear Data Library Version 3 Revision-2: JENDL-3.2," Journal of Nuclear Science and Technology, 32[12], P1259-1271 (1995).
6. T.Nakagawa, "Summary of JENDL-2 General Purpose File" , JAERI-M 84-103, JAERI (1984).
7. "DIF3D 7.0 : Code System for Solving Finite Difference Diffusion Theory Problems," RSIC, CCC-649, (1997)
8. M.Nakagawa and K.Tuchihashi, "SLAROM: A Code for Cell Homogenization Calculation of Fast Reactor," JAERI 1294, JAERI (1989)
9. T.Sakurai, et al., "Measurement and Analysis of Breeding Indices of U-238 Capture to Pu-239 Fission Rate Ratio and U-238 capture to U-235 Fission Rate Ratios at Fast Critical Assembly," JAERI-Research 95-054, JAERI (1989).
10. H.Akima, "Interpolation and Smooth Curve Fitting Based on Local Procedures," Communications of the ACM, Vol.15, Num.10, Oct. (1972), p914.